

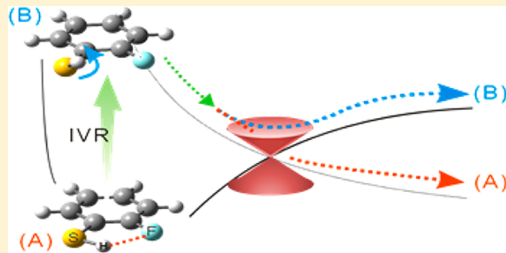
# Dynamic Role of the Intramolecular Hydrogen Bonding in Nonadiabatic Chemistry Revealed in the UV Photodissociation Reactions of 2-Fluorothiophenol and 2-Chlorothiophenol

Songhee Han,<sup>†,‡</sup> Hyun Sik You,<sup>†</sup> So-Yeon Kim, and Sang Kyu Kim<sup>\*</sup>

Department of Chemistry, KAIST, Daejeon 305-701, Republic of Korea

 Supporting Information

**ABSTRACT:** The dynamic interplay between the intramolecular hydrogen bonding and intramolecular vibrational redistribution is found to be critical in nonadiabatic reaction dynamics. Herein, it has been demonstrated that the molecular planarity, directed by the intramolecular hydrogen bonding, plays an important role in the nonadiabatic passage of the reactive flux at the conical intersection in the photodissociation reactions of 2-fluorothiophenol and 2-chlorothiophenol. As the internal energy increases in the excited state, the intramolecular hydrogen bonding of 2-fluorothiophenol loosens. The floppiness brought into the molecular structure then modifies the dynamic path of the reactive flux, leading to the diminishment of the nonadiabatic transition probability at the conical intersection. On the contrary, for 2-chlorothiophenol having the relatively stronger intramolecular hydrogen bonding, the reactive flux seems to retain the molecular planarity even with the increase of the internal energy as manifested by the constant nonadiabatic transition probability over the wide range of the  $S_1$  internal energy. The effect of the intramolecular hydrogen bonding on the molecular structure and its relation to the nonadiabatic dynamics along the tunneling path has been experimentally demonstrated.



## INTRODUCTION

Hydrogen bonding is an essential component in chemistry and biology.<sup>1–5</sup> It directs the molecular structure and controls dynamics of chemical reactions in many circumstances. At the fundamental level, the role of the hydrogen bonding has long been investigated in the molecular cluster system. Therein, the effect of hydrogen bonding on the electronic/nuclear configurations and chemical reactions have been both extensively and intensively studied for decades.<sup>6–10</sup> In this contribution, we have specifically investigated the dynamic role of the intramolecular hydrogen bonding in the nonadiabatic transition. Nonadiabatic transitions are ubiquitous in nature, and it is well accepted that the multidimensional conical intersection seam is a dynamic bottleneck in such processes.<sup>11–30</sup> Accordingly, as the reactive flux passes in closer proximity to the conical intersection, the nonadiabatic transition becomes more probable. Therefore, the nuclear configuration of the initial reactive flux on the excited state should be one of the most critical factors in the determination of the nonadiabatic transition probability along the reaction pathway. The intriguing point of this work is that the structure of the molecule having the intramolecular hydrogen bonding is dynamically manipulated by the internal energy excitation, eventually modifying the nonadiabatic transition probability at the conical intersection.

Recently, it has been reported that the nonadiabatic transition probability at the conical intersection can be precisely estimated by measuring the kinetic energy distribution of the nascent fragment from the UV photodissociation of thiophene-

nol<sup>24,31–35</sup> or thioanisole.<sup>18,36</sup> As a final product, the phenylthiyl radical ( $C_6H_5S\cdot$ ) is produced as either the one in the ground ( $\tilde{X}$ ) or excited ( $\tilde{A}$ ) state. Interestingly, a  $C_6H_5S\cdot(\tilde{X})$  fragment is yielded from the nonadiabatic transition, whereas the  $C_6H_5S\cdot(\tilde{A})$  fragment is the product of the adiabatic reaction pathway. Namely, along the S–H bond elongation coordinate of thiophenol, two conical intersections are encountered. The first conical intersection is generated by the crossing of the bound  $S_1$  and repulsive  $S_2$  states, yielding the  $S_1/S_2$  conical intersection. At a later stage, the diabatic  $S_0$  state correlating to the  $H + C_6H_5S\cdot(\tilde{A})$  channel crosses with the repulsive  $S_2$  state, which is diabolically correlated to the  $H + C_6H_5S\cdot(\tilde{X})$  channel to yield the  $S_0/S_2$  conical intersection, as shown in Figure 1. In both cases, the surface crossing occurs at the planar geometry. The nonadiabatic transition probability, therefore, should be strongly sensitive to the nuclear configuration especially in terms of the molecular planarity. Actually, it was shown in our earlier report that the nonadiabatic transition probability could be manipulated by the chemical substitution of thiophenol at the *para* position.<sup>37</sup> When the methoxy ( $-\text{OCH}_3$ ) group is substituted at the *para* position of thiophenol, for instance, the molecule adopts the nonplanar geometry with a dihedral angle of  $\sim 80^\circ$  between the plane containing the SH bond axis and that of the benzene moiety. The instant excitation to the repulsive  $S_2$  state at this nonplanar nuclear configuration then diminishes the nonadiabatic transition probability in the *p*-

Received: June 9, 2014

Published: August 6, 2014



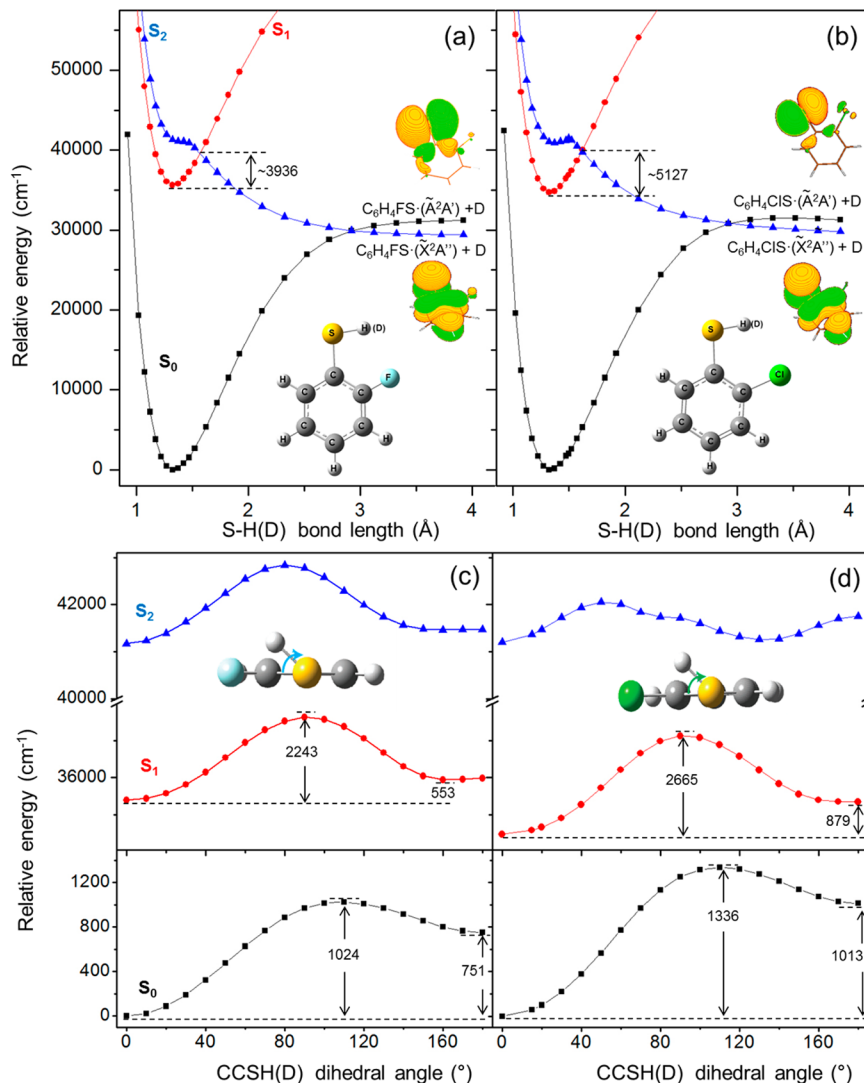


**Figure 1.** Three lowest diabatic potential energy curves ( $S_0$ ,  $S_1$ ,  $S_2$ ) of (a) 2-fluorothiophenol and (b) 2-chlorothiophenol along the S–H bond elongation coordinate at the planar geometry, obtained by the CASPT2//SA3-CASSCF(10,9)/6-311+G(3df,3pd) calculation. The PECs along CCSH dihedral angle for (c) 2-fluorothiophenol and (d) 2-chlorothiophenol are calculated by the CASPT2//SA3-CASSCF(12,11)/6-311+G(3df,3pd) method. See the text for details.

methoxythiophenol, giving a ~10% yield of the  $C_6H_5S\cdot(\tilde{X})$  fragment, which is much smaller than the ~45% yield from the thiophenol dissociation at the same excitation energy. This experimental result has also been confirmed by the Ashfold group.<sup>38</sup> They also examined the  $S_1$ -state nonadiabatic dynamics of several *para*-substituted thiophenols as a function of the internal energy, finding that the intramolecular vibrational redistribution (IVR) may play a significant role in guiding the reaction pathway around the conical intersection seam.

Herein, we have chosen 2-fluorothiophenol (2-FTP) and 2-chlorothiophenol (2-CTP) to investigate the dynamic role of the intramolecular hydrogen bonding in nonadiabatic chemistry. In these systems, the F or Cl atom at the ortho position makes the intramolecular hydrogen bonding with the adjacent SH moiety, which helps the molecule retain the planar geometry. Interestingly, because of the existence of the intramolecular hydrogen bonding, the molecular planarity becomes a dynamic variable in nonadiabatic reaction dynamics. In other words, the vibrational excitation may tighten or loosen the intramolecular hydrogen bonding, and thus, the dynamic

interplay between the vibrational energy flow and the intramolecular hydrogen bonding plays a significant role in nonadiabatic reaction dynamics.

## EXPERIMENTAL SECTION

The experimental method used in the present study has been described in detail elsewhere.<sup>32,34</sup> Briefly, 2-FTP-*d*<sub>1</sub> and 2-CTP-*d*<sub>1</sub> were prepared by mixing D<sub>2</sub>O with 2-FTP (TCI, >95.5%) or 2-CTP (TCI, >97.0%) dissolved in ether. The mixture was stirred vigorously before the separation and isolation of the isotopically substituted sample. This procedure was repeated several times. For the resonantly enhanced two-photon ionization (R2PI) spectroscopy, the sample was heated to 53 °C for 2-FTP-*d*<sub>1</sub> and 68 °C for 2-CTP-*d*<sub>1</sub>, mixed with the Ar carrier gas to be expanded through a nozzle orifice (General Vale series 9, 0.5 mm diameter) into a vacuum with a backing pressure of ~1 atm. R2PI spectra were obtained by monitoring the parent molecular ion as a function of the excitation wavelength in the range of 281–265 nm for 2-FTP-*d*<sub>1</sub> and 289–275 nm for 2-CTP-*d*<sub>1</sub>. To measure the translational

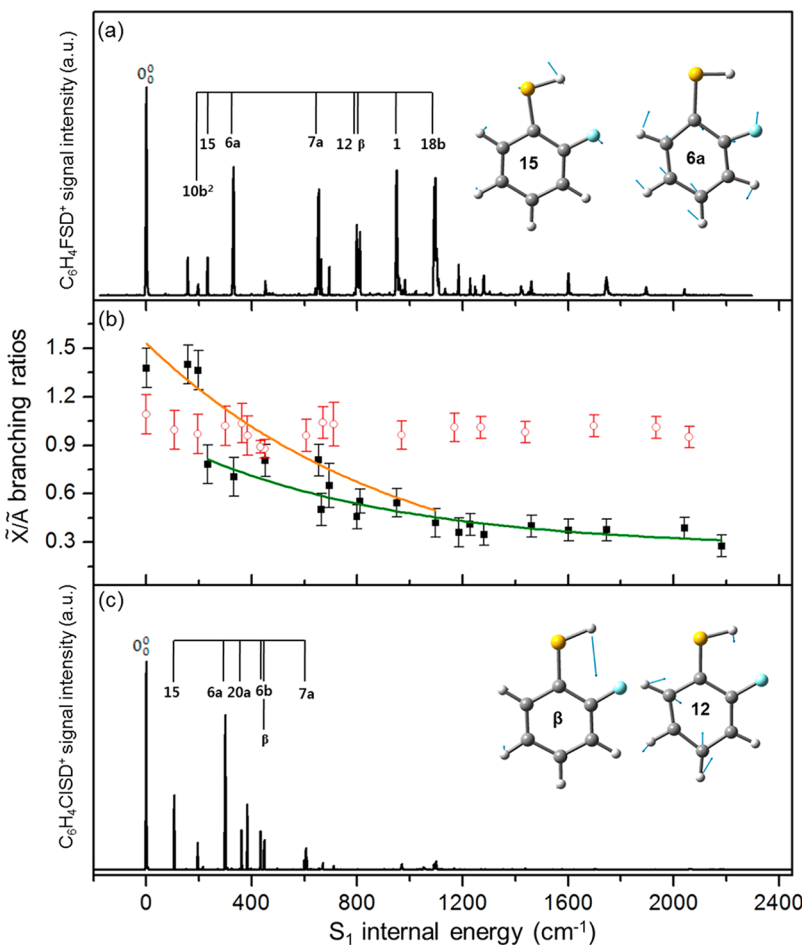


**Figure 2.** R2PI spectra of (a) 2-fluorothiophenol-*d*<sub>1</sub> and (c) 2-chlorothiophenol-*d*<sub>1</sub> with appropriate vibrational mode assignments. The experimentally estimated  $\tilde{X}/\tilde{A}$  branching ratios are plotted as a function of the  $S_1$  internal energy for 2-fluorothiophenol-*d*<sub>1</sub> (black filled squares) and 2-chlorothiophenol-*d*<sub>1</sub> (red open circles) (b). Nuclear displacement vectors of some notable vibrational modes of 2-fluorothiophenol-*d*<sub>1</sub> are also shown in the inset. Exponential curves are drawn for the visual aid.

energy and angular distributions of the D atom fragment, the velocity map ion imaging technique was employed.<sup>39</sup> When the image was taken, the pump laser wavelength was fixed at a particular  $S_1$  vibronic band, whereas the probe laser was continually scanned over the entire Doppler width of the nascent D atom fragment. Three-dimensional images were obtained by the reconstruction of raw images by using the BASEX algorithm.<sup>40</sup> The polarization of the pump laser was parallel to the detector plane. The total translational energy distributions were obtained by consideration of the Jacobian factor.

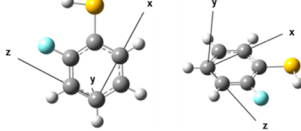
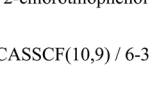
**Computational Details.** The state averaged complete active space self-consistent field (SA3-CASSCF)<sup>41,42</sup> and second-order multireference perturbation theory (CASPT2)<sup>43</sup> methods were used to construct the diabatic potential energy curves (PECs) of 2-fluorothiophenol and 2-chlorothiophenol in the  $S_0$ ,  $S_1$ , and  $S_2$  states. Here, either the S–H(D) bond length or CCSH(D) dihedral angle was varied, while the remaining geometrical parameters were fixed at those of the minimum energy structure of  $S_0$  state. Along the S–H(D) bond elongation coordinate, the active space used in the CASSCF calculations was CAS(10,9). Here, nine orbitals used include three pairs of  $\pi/\pi^*$  orbitals of ring, a nonbonding *p*-orbital of sulfur,  $\sigma_{S-H}$ , and  $\sigma^*_{S-H}$ . The  $\sigma_{C-S}$  and  $\sigma^*_{C-S}$  orbitals were added to provide an active space of CAS(12,11) for the

construction of PECs along the CCSH(D) dihedral angle (Table S1, Supporting Information). The basis set of 6-311+G(3df,3pd) was used for CASSCF calculations. The optimized structures and vibrational frequencies of  $S_0$  and  $S_1$  states were calculated by using the DFT (B3LYP) method<sup>44</sup> with a 6-311++G(3df,3pd) basis set in order to be used in the Franck–Condon (FC) analysis.<sup>45,46</sup> The natural bond orbital (NBO) analysis<sup>47</sup> was performed for the  $S_0$  molecular structures, which were fully optimized at several CCSD dihedral angles. Vertical excitation energies were obtained using the (TD)-DFT and CASPT2 methods with appropriate basis sets. All CASSCF and CASPT2 calculations were performed with MOLPRO (version 2010.1),<sup>48</sup> while the DFT calculations were carried out using the Gaussian 09 program package.<sup>49</sup>

## RESULTS AND DISCUSSION

**S<sub>1</sub> Vibronic Structures and Energetics of 2-Fluorothiophenol and 2-Chlorothiophenol.** Unlike thiophenol of which the  $S_1$  lifetime is known to be extremely short, the lifetimes of the  $S_1$  states of 2-FTP and 2-CTP seem to be sufficiently long to obtain well-resolved R2PI spectra of the  $S_1$ – $S_0$  transitions, as shown in Figure 2. Actually, the observation of the sharp  $S_1$  vibronic bands in the R2PI spectra of 2-FTP and 2-CTP is somewhat surprising, as it is reported in previously

**Table 1.** Calculated Vertical Excitation Energies, Oscillator Strengths, and Transition Dipole Moments<sup>a</sup>

| State   | Excitation wavelength | Oscillator strength | Transition dipole moment ( $\mu$ ) |         |         |  |  |
|---|-----------------------|---------------------|------------------------------------|---------|---------|--|--|
|   |                       |                     | $\mu_x$                            | $\mu_y$ | $\mu_z$ |  |  |
| <br>2-fluorothiophenol   |                       |                     |                                    |         |         |  |  |
| CASPT2//SA4-CASSCF(10,9) / 6-311++G(3df,3pd)  |                       |                     |                                    |         |         |  |  |
| State 1( $\pi\pi^*$ )   | 281.99 nm             | 0.00497             | 0.0386                             | 0.00    | -0.2113 |  |  |
| State 2( $n_{\pi}\sigma^*$ )  | 240.00 nm             | 0.00168             | 0.00                               | -0.1153 | 0.00    |  |  |
| State 3( $\pi\pi^*$ )   | 232.90 nm             | 0.24663             | -0.0495                            | 0.00    | -1.3743 |  |  |
| TD-HCTH/6-311++G(3df,3pd)   |                       |                     |                                    |         |         |  |  |
| State 1( $\pi\pi^*$ )   | 280.27 nm             | 0.0351              | 0.4843                             | -0.2985 | 0.0000  |  |  |
| State 2( $n_{\pi}\sigma^*$ )  | 255.52 nm             | 0.0036              | 0.0000                             | 0.0000  | 0.1739  |  |  |
| State 3( $\pi\pi^*$ )   | 250.08 nm             | 0.2087              | 0.6447                             | -1.1413 | 0.0000  |  |  |
| <br>2-chlorothiophenol |                       |                     |                                    |         |         |  |  |
| CASPT2//SA4-CASSCF(10,9) / 6-311++G(3df,3pd)  |                       |                     |                                    |         |         |  |  |
| State 1( $\pi\pi^*$ )   | 290.19 nm             | 0.00022             | 0.0363                             | 0.0000  | -0.0279 |  |  |
| State 2( $n_{\pi}\sigma^*$ )  | 241.52 nm             | 0.00153             | 0.0000                             | -0.1104 | 0.0000  |  |  |
| State 3( $\pi\pi^*$ )   | 240.23 nm             | 0.24811             | -0.6685                            | 0.0000  | -1.2309 |  |  |
| TD-HCTH/6-311++G(3df,3pd)   |                       |                     |                                    |         |         |  |  |
| State 1( $\pi\pi^*$ )   | 290.19 nm             | 0.0169              | 0.3183                             | -0.2461 | 0.0000  |  |  |
| State 2( $n_{\pi}\sigma^*$ )  | 267.39 nm             | 0.0004              | 0.0000                             | 0.0000  | 0.0603  |  |  |
| State 3( $\pi\pi^*$ )   | 256.42 nm             | 0.1935              | -0.9687                            | -0.8336 | 0.0000  |  |  |

<sup>a</sup>Cartesian axes for the transition dipole moments are also given for the molecular structure obtained via the CASPT2 method. See the Supporting Information for the Cartesian axes obtained via TD-HCTH method.

studies that the S–H(D) bond dissociation of thiophenol is extremely fast even at the  $S_1$  origin.<sup>33</sup> The much longer  $S_1$  lifetime of 2-FTP and 2-CTP should then originate from their different electronic structures compared to thiophenol. Indeed,

the vertical energy gap between  $S_1$  and  $S_2$  states is predicted to be 6205 (3456)  $\text{cm}^{-1}$  for 2-FTP from the CASPT2 (TD-HCTH) calculation. For 2-CTP, it is 6944 (2939)  $\text{cm}^{-1}$  from the CASPT2 (TD-HCTH) calculation, as shown in Table 1.

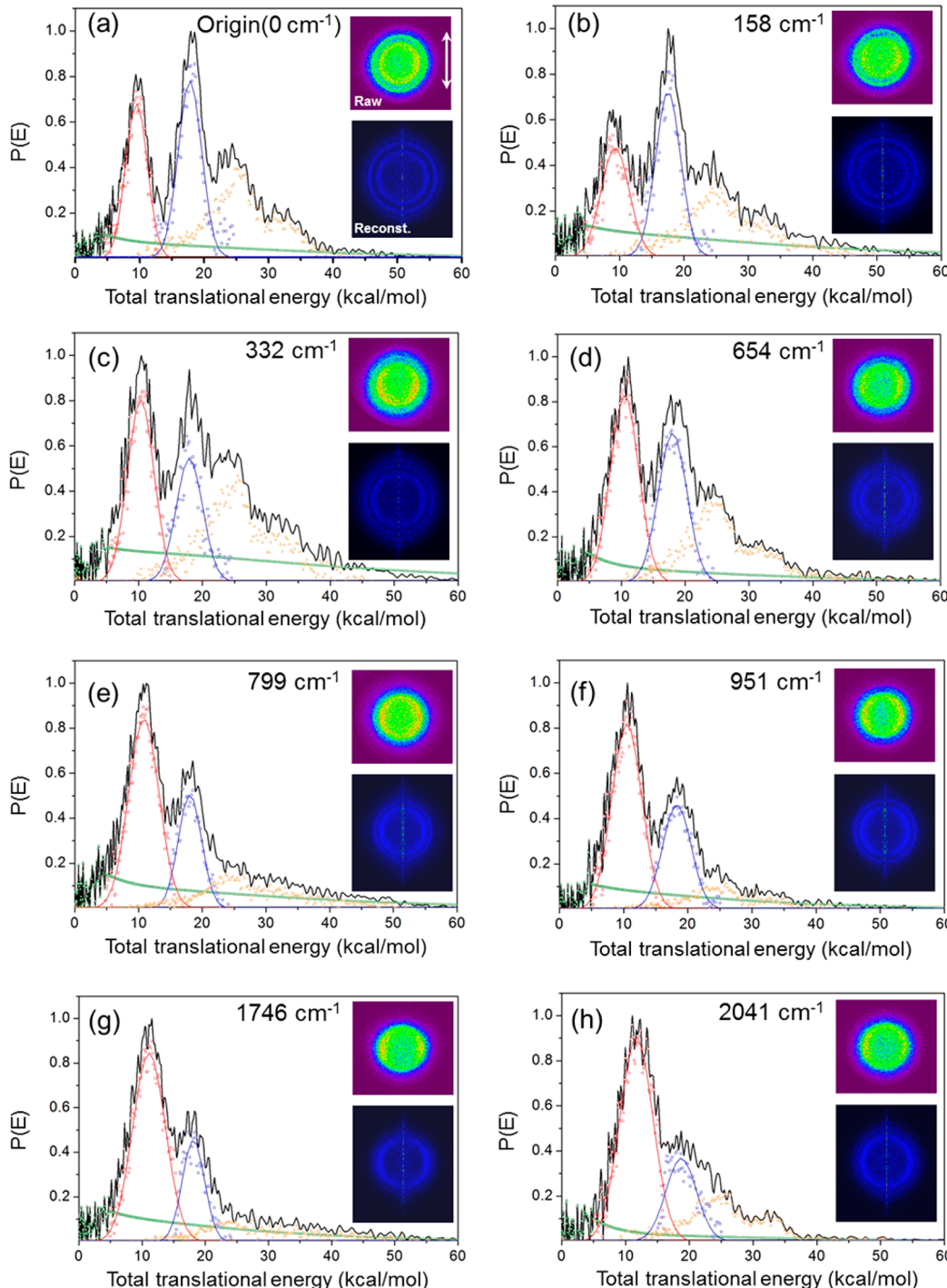


**Figure 3.** Total translational energy distributions from the S–D bond dissociation of 2-fluorothiophenol-*d*<sub>1</sub> at several S<sub>1</sub> internal energies. The white arrow indicates the polarization direction of the pump pulse. Raw (upper) and reconstructed (lower) images are shown. Contributions from the probe laser only (orange) and other Boltzmann-like background (green) are subtracted in the  $\tilde{X}/\tilde{\Lambda}$  branching ratio estimation. Fitting equations for the background are explained in the Supporting Information.

The vertical excitation energy gap is strongly dependent on the calculation method, and yet it is clear that the S<sub>1</sub>–S<sub>2</sub> vertical energy gap of 2-FTP or 2-CTP is much larger than that of thiophenol, which is calculated to be 3886 (1291) cm<sup>-1</sup> using the CASPT2 (TD-HCTH) method.<sup>32</sup> This indicates that the S<sub>1</sub>/S<sub>2</sub> coupling starts much earlier for thiophenol compared to 2-FTP or 2-CTP. One can estimate the upper limit of the adiabatic reaction barrier for the S–H(D) dissociation from the curve crossing point of the bound S<sub>1</sub> and repulsive S<sub>2</sub> along the

S–H elongation coordinate. According to the potential energy curves calculated at the CASPT2 level, the upper limit of the adiabatic reaction barrier is found to be ~3936 or ~5127 cm<sup>-1</sup> for 2-FTP or 2-CTP, respectively, which is much higher than the value of 2085 cm<sup>-1</sup> predicted for thiophenol.<sup>35</sup> These somewhat large barriers to the S–H bond dissociation clearly explain why the S<sub>1</sub> lifetime of 2-FTP or 2-CTP is much longer than that of thiophenol.

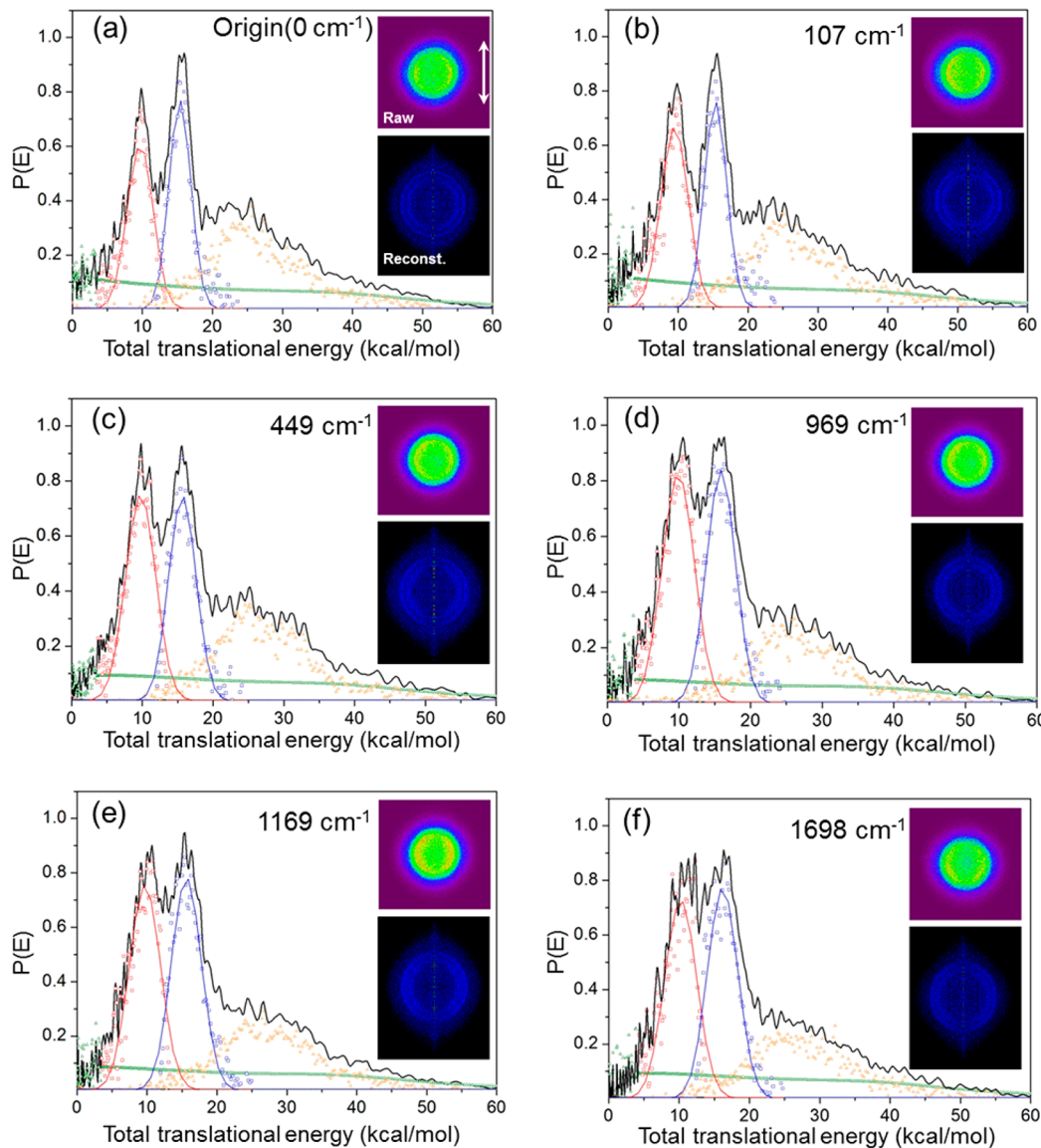


**Figure 4.** Total translational energy distributions from the S–D bond dissociation of 2-chlorothiophenol- $d_1$  at several  $S_1$  internal energies. See the figure caption of Figure 3 for the remaining details.

The  $S_1-S_0$  spectral origin band is observed at 35 555 or 34 627  $\text{cm}^{-1}$  for 2-FTP or 2-CTP, respectively. For 2-FTP- $d_1$  ( $\text{C}_6\text{H}_4\text{F-SD}$ ) or 2-CTP- $d_1$  ( $\text{C}_6\text{H}_4\text{Cl-SD}$ ), the origin is found at 35 547 or 34 620  $\text{cm}^{-1}$ , respectively. The  $S_1$  vibronic bands of undeuterated and deuterated species of both 2-FTP and 2-CTP have been assigned using the Franck–Condon analysis based on DFT calculations. As the excited state calculation for vibrational frequencies is often unreliable, a slow electron velocity imaging (SEVI) experiment was carried out. According to the propensity rule of  $\Delta v = 0$ , the most strongly observed  $D_0$  (cationic ground state) band represents the nature of the  $S_1$  vibronic state used as an intermediate state in the corresponding ( $1 + 1'$ ) SEVI spectrum. Therefore, the proper assignment of the  $D_0$  vibrational bands from the comparison with the *ab initio* calculated values leads to the appropriate assignment for  $S_1$  vibronic bands. For both 2-FTP and 2-CTP, the cis form in which the F-HS or Cl-HS intramolecular hydrogen bonding plays a critical role in retaining the molecular planarity is found to be the most stable one. Namely, the cis form in the ground electronic state is predicted to be more

stable compared to trans by 751 (302) or 1013 (79)  $\text{cm}^{-1}$  by the CASPT2 (DFT) calculation for 2-FTP or 2-CTP, respectively. The relative stabilization energies calculated by the two methods are quite different. Obviously, the  $D_0-S_1-S_0$  transition induces little structural change as evidenced by the observation of the strong origin band in each transition. The mode assignments for most  $S_1$  vibronic bands of 2-FTP and 2-CTP are then straightforward. It is noteworthy, though, that the vibrational frequencies associated with  $\text{C}_{(6)}\text{SH}$  bending (15) and  $\beta$  modes are not reproduced very well by the calculation. These modes are strongly dependent on the deuterium exchange of the SH moiety, and the spectral assignment is secured from our spectroscopic comparison between undeuterated and deuterated species. For the  $\beta$  mode, for instance, its frequency is found at 892 (900) and 925 (942)  $\text{cm}^{-1}$  for  $S_1$  and  $D_0$  states of 2-FTP, respectively, where numbers in parentheses are DFT values. Interestingly, however, the experimental frequency for  $\beta$  is not shifted much by the SH/SD substitution to give 811 and 899  $\text{cm}^{-1}$  for  $S_1$  and  $D_0$  of 2-FTP- $d_1$ , respectively, whereas it is predicted to be 672 or 702  $\text{cm}^{-1}$  from

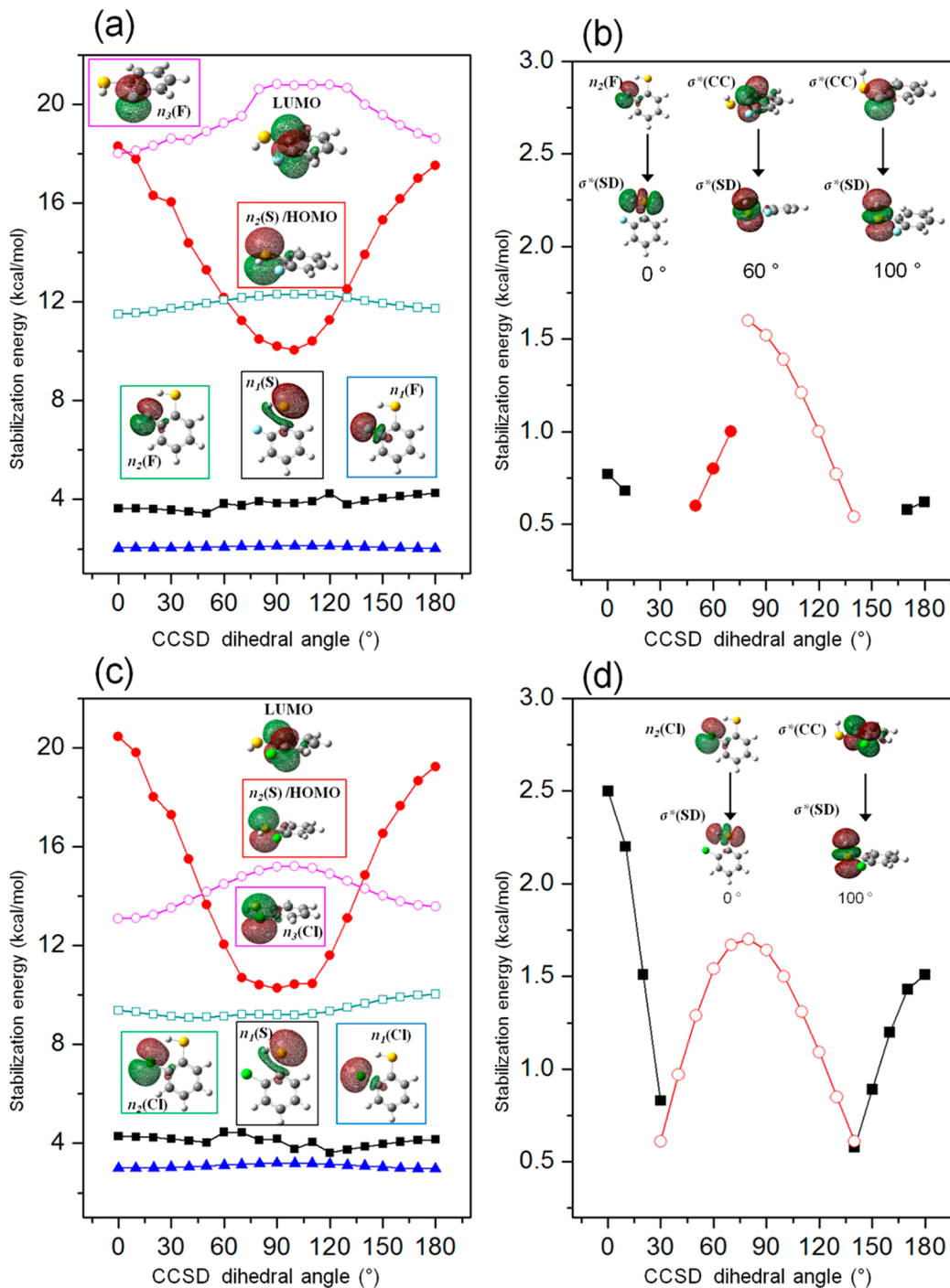


**Figure 5.** Stabilization energies of 2-fluorothiophenol- $d_1$  (a,b) and 2-chlorothiophenol- $d_1$  (c,d) obtained by the NBO analysis calculated as a function of CCSD dihedral angle. On the left, the stabilization energies correspond to the orbital interactions between LUMO and nonbonding orbitals of  $n_1$ (F or Cl) (blue filled triangles),  $n_2$ (F or Cl) (green open squares),  $n_3$ (F or Cl) (magenta open circles),  $n_1$ (S) (black filled squares), and  $n_2$ (S) (red filled circles). On the right, the stabilization energies induced from the interaction between S–D bond antibonding ( $\sigma^*(SD)$ ) and  $n_2$ (F or Cl) (black filled squares) or  $\pi^*(C–C)$  (red filled and empty circles) orbitals are depicted.

DFT calculations, respectively. This large discrepancy in the isotopic shift of the vibrational energy between the experiment and calculation reflects the lack of the understanding of intramolecular hydrogen bonding in terms of force constants and associated anharmonicity.

**Nonadiabatic Transition Probability as a Function of the Internal Energy: Dynamic Interplay between IVR and Intramolecular Hydrogen Bonding.** Velocity-map ion images of  $D^+$  from 2-FTP- $d_1$  and 2-CTP- $d_1$  are obtained at the

excitation energies in the 281–265 and 289–275 nm regions, respectively. Because of the efficient D atom fragmentation at the probe wavelength of 243.1 nm, the background signal due to only the probe laser persists in all images, as shown in Figures 3 and 4. In the D fragment translational energy distributions, after the subtraction of the background signal, two distinct Gaussian-shaped distributions associated with the  $\tilde{X}$  and  $\tilde{A}$  states of the  $F–C_6H_4S$  (or  $Cl–C_6H_4S$ ) radical are clearly resolved to give the precise  $\tilde{X}/\tilde{A}$  branching ratio at the given  $S_1$

excitation wavelength. For instance, the Gaussian-shaped distributions that peaked at the translational energies of  $\sim 10$  or  $\sim 18$  kcal/mol represent the  $\tilde{A}$  or  $\tilde{X}$  state of the F-C<sub>6</sub>H<sub>4</sub>S radical, respectively, whereas those associated with the  $\tilde{A}$  or  $\tilde{X}$  state of the Cl-C<sub>6</sub>H<sub>4</sub>S radical peaked at  $\sim 10$  and  $\sim 16$  kcal/mol, respectively. The energy gap between two peaks in the translational energy distribution is  $\sim 2800$  and  $\sim 2100$  cm<sup>-1</sup> for the F-C<sub>6</sub>H<sub>4</sub>S or Cl-C<sub>6</sub>H<sub>4</sub>S radical, respectively. These values are consistent with the calculated (CASPT2) values of 2752 and 2148 cm<sup>-1</sup> for the  $\tilde{A}-\tilde{X}$  vertical energy gap of the F-C<sub>6</sub>H<sub>4</sub>S or Cl-C<sub>6</sub>H<sub>4</sub>S radical, respectively. The relatively larger  $\tilde{A}-\tilde{X}$  energy gap of the F-C<sub>6</sub>H<sub>4</sub>S radical indicates that the  $\pi$ -orbital conjugation of the phenyl moiety with adjacent sulfur and halogen atoms in F-C<sub>6</sub>H<sub>4</sub>S is more significant than that in the Cl-C<sub>6</sub>H<sub>4</sub>S radical. This rather large difference in the  $\tilde{A}-\tilde{X}$  energy gap of these two radicals is closely related to the difference in the strength of the intramolecular hydrogen bonding.

In thiophenol, the S<sub>1</sub> vibronic states are quasi-bound due to ultrafast S–H bond ruptures in the excited state. The initially prepared reactive flux at S<sub>1</sub>, therefore, is likely to maintain its nuclear configuration except its change along the elongating S–H bond axis. Namely, energy randomization does not occur prior to the ultrafast S–H bond cleavage. Therefore, with increasing the S<sub>1</sub> internal energy, unless the selected vibronic mode is strongly coupled to the reaction coordinate in terms of the nonadiabatic transition, the nonadiabatic transition probability is not expected to change significantly as a function of the S<sub>1</sub> internal energy. This is quite consistent with the recent experimental report.<sup>33</sup> For both 2-FTP-d<sub>1</sub> and 2-CTP-d<sub>1</sub>, however, the situation is different. Namely, the S<sub>1</sub> lifetimes of those molecules are quite long to allow for the energy randomization before the S–D bond breaking event. The most critical geometrical factor in the nonadiabatic transition seems to be the molecular planarity as both the S<sub>1</sub>/S<sub>2</sub> and S<sub>0</sub>/S<sub>2</sub> conical intersections adopt planar geometry.

The  $\tilde{X}/\tilde{A}$  product branching ratio, representing the nonadiabatic transition probability, is estimated from the relative ratio of two deconvoluted Gaussian-shaped distributions after the background subtraction, as shown in Figure 2. The  $\tilde{X}/\tilde{A}$  branching ratio of 2-FTP-d<sub>1</sub> at its S<sub>1</sub> origin is measured to be  $\sim 1.4$ , indicating that the nonadiabatic transition probability at the S<sub>0</sub>/S<sub>2</sub> conical intersection is quite significant. However, as the S<sub>1</sub> internal energy increases, the  $\tilde{X}/\tilde{A}$  ratio sharply decreases to  $\sim 0.4$  at  $\sim 1200$  cm<sup>-1</sup> above the S<sub>1</sub> origin and remains constant at the higher excitation energies. However, the  $\tilde{X}/\tilde{A}$  branching ratio from 2-CTP-d<sub>1</sub> at the S<sub>1</sub> origin is  $\sim 1.05$ , and it is found to be more or less constant up to  $\sim 2000$  cm<sup>-1</sup> above the origin. The different nonadiabatic behaviors of 2-FTP-d<sub>1</sub> and 2-CTP-d<sub>1</sub> with increasing the S<sub>1</sub> internal energy are quite remarkable as the S–D bond dissociation pathways of two molecules are not expected to be much different.

The sharp decrease of the  $\tilde{X}/\tilde{A}$  branching ratio observed for 2-FTP-d<sub>1</sub> may then indicate that the reaction path becomes nonplanar with increasing the S<sub>1</sub> internal energy. At the S<sub>1</sub> zero-point energy level, the S–D bond dissociation occurs via tunneling through the barrier whose top corresponds to the S<sub>1</sub>/S<sub>2</sub> conical intersection. The reactive flux on the repulsive S<sub>2</sub> state then partly undergoes the nonadiabatic transition at the S<sub>0</sub>/S<sub>2</sub> conical intersection to produce the ground state of the F-C<sub>6</sub>H<sub>4</sub>S radical. The abrupt decrease of the  $\tilde{X}/\tilde{A}$  branching ratio to  $\sim 0.8$  (from  $\sim 1.4$  at the S<sub>1</sub> origin) is observed at the 233 cm<sup>-1</sup> vibronic band associated with the CSD in-plane bending.

This mode may contribute to the weakening of the F···D intramolecular hydrogen bond, leading to the decrease of the CCSD torsional barrier height, which is intrinsically dynamic and thus sensitive to the relevant vibrational activation. As the torsional barrier is lowered, the reactive flux becomes more dispersed along the out-of-plane CCSD torsional angle. This will make the reactive flux take the tunneling path through the reaction barrier at the nonplanar geometry. The effective barrier for the S–D tunneling will be adiabatically lowered at the nonplanar geometry compared to that at the planar geometry. Nonadiabatic transition probability of the reactive flux tunneled at the nonplanar geometry will be diminished at the S<sub>0</sub>/S<sub>2</sub> conical intersection, yielding a smaller  $\tilde{X}/\tilde{A}$  branching ratio. Similar mode effects are observed for 6a, 12, and  $\beta$  modes at 332, 799, and 811 cm<sup>-1</sup>, respectively. For other vibronic modes, the  $\tilde{X}/\tilde{A}$  branching ratio shows a gradual decrease with increasing the S<sub>1</sub> internal energy, yielding  $\sim 0.4$  at  $\sim 1200$  cm<sup>-1</sup> above the origin. This may indicate that the F···D intramolecular hydrogen bond becomes completely loosened at  $\sim 1200$  cm<sup>-1</sup> or higher above the origin, giving the higher probability for the nonplanar adiabatic passage of the reactive flux at the S<sub>0</sub>/S<sub>2</sub> conical intersection. The opposite behavior of the  $\tilde{X}/\tilde{A}$  branching ratio as a function of the S<sub>1</sub> internal energy for 2-CTP-d<sub>1</sub> seems to originate from its stronger Cl···D intramolecular hydrogen bond compared to the F···D intramolecular hydrogen bond of 2-FTP-d<sub>1</sub>. Actually, according to the CASPT2 calculation, the CCSD torsional barrier height of 2-CTP-d<sub>1</sub> is predicted to be  $\sim 400$  cm<sup>-1</sup> higher than that of 2-FTP-d<sub>1</sub> in the S<sub>1</sub> state, Figure 1. This suggests that the relative stronger intramolecular hydrogen bonding of 2-CTP-d<sub>1</sub> makes the molecule retain its planarity, even at the high internal energy excitation, yielding a  $\tilde{X}/\tilde{A}$  branching ratio that remains constant up to  $\sim 2000$  cm<sup>-1</sup> above the origin.

Natural bond orbital (NBO) analysis<sup>50,51</sup> helps explain our experimental results. The stabilization energies induced from the orbital overlap between the lowest-occupied molecular orbital (LUMO) and nonbonding orbitals, which are related to the S<sub>1</sub> potential energy, are given as a function of the CCSD dihedral angle in Figure 5. The stabilization effect is found to be most significant for the interaction with the highest-occupied molecular orbital (HOMO) corresponding to the sulfur nonbonding orbital and one of three nonbonding orbitals of F ( $n_3(F)$ ) or Cl ( $n_3(Cl)$ ). The HOMO–LUMO interaction energy is strongly dependent on the CCSD dihedral angle, peaking at the planar geometry for both 2-FTP and 2-CTP. The difference between the stabilization energy at the CCSD angle of 0° and that at 90°, however, is calculated to be larger for 2-CTP compared to that of 2-FTP. This explains why the CCSD torsional barrier height is expected to be larger for 2-CTP compared to that of 2-FTP. The  $n_3(F)$ -LUMO or  $n_3(Cl)$ -LUMO stabilization energy, however, is calculated to be larger at the nonplanar geometry compared to that at the planar geometry. The corresponding stabilization energy increment as the CCSD angle is changed to 90° from 0° is less significant for both molecules. The calculation predicts that the contribution of the  $n_3(F)$ -LUMO interaction to the stability of the nonplanar geometry of 2-FTP is relatively larger compared to that of the  $n_3(Cl)$ -LUMO stabilization energy in 2-CTP. This also supports that the Cl···D intramolecular hydrogen bond of 2-CTP is stronger than the F···D intramolecular hydrogen bond of 2-FTP. The orbital interactions responsible for the intramolecular hydrogen bonding along the S–D bond dissociation pathway are those between  $n_2(F)$  (or  $n_2(Cl)$ )

and  $\sigma^*(SD)$  for 2-FTP (or 2-CTP). As clearly shown in Figure 5, the planar geometry is largely favored by the  $n_2(Cl)-\sigma^*(SD)$  orbital interaction for 2-CTP, whereas the contribution of the  $n_2(F)-\sigma^*(SD)$  interaction is negligible to the stabilization of the planar structure of 2-FTP.

## CONCLUSIONS

Herein, photodissociation dynamics of 2-fluorothiophenol and 2-chlorothiophenol have been investigated to elucidate the dynamic interplay between the intramolecular hydrogen bonding and intramolecular vibrational redistribution in the vicinity of the conical intersection. Unlike the case of thiophenol where the S–H bond rupture takes place promptly, the  $S_1$  excited-state lifetimes of 2-FTP and 2-CTP are quite long and the intramolecular vibrational redistribution plays a critical role in the determination of the dissociation pathway. In particular, for 2-FTP, the dissociation path becomes adiabatic as the  $S_1$  internal energy increases, indicating that the reactive flux prefers taking the tunneling path through the adiabatically lowered reaction barrier at the nonplanar geometry with an increase in the internal energy. In 2-CTP, however, due to the relatively stronger intramolecular hydrogen bonding, the nonadiabatic transition probability remains significant, even at high internal energies. Herein, we have demonstrated that the nonadiabatic transition probability can be controlled based on the fundamental understanding of the dynamic interplay between the vibrational energy flow and molecular structure mediated by the intramolecular hydrogen bonding.

## ASSOCIATED CONTENT

### Supporting Information

Molecular orbitals used for the CASSCF calculations, Cartesian axes of the molecular structure obtained by TD-HCTH calculation, R2PI and Franck–Condon simulation spectra, SEVI spectroscopy of 2-fluorothiophenol and 2-chlorothiophenol, potential energy curves along CCSH(D) dihedral angle, fitting of total translational energy distributions and determination of  $\tilde{X}/\tilde{A}$  branching ratios, the calculation of energy gaps between  $\tilde{X}$  and  $\tilde{A}$  states of 2-fluorophenylthiyl and 2-chlorophenylthiyl radicals, and total translational energy distributions for the dissociation of 2-fluorothiophenol- $d_1$ . This material is available free of charge via the Internet at <http://pubs.acs.org>.

## AUTHOR INFORMATION

### Corresponding Author

<sup>\*(S.K.K.)</sup> E-mail: sangkyukim@kaist.ac.kr. Tel: (+)82-42-350-2843.

### Present Address

<sup>‡</sup>(S.H.) Max Born Institute for Nonlinear Optics and Short Pulse Spectroscopy in Berlin Research Association, Max-Born-Str. 2 A 12489, Berlin, Germany.

### Author Contributions

<sup>†</sup>S.H. and H.S.Y. contributed equally to this work.

### Notes

The authors declare no competing financial interest.

## ACKNOWLEDGMENTS

This work has been supported by Grants of National Research Foundation (2012-0005607 and SRC 2012-0000779). S.H. appreciates the support of the National Junior Research Fellowship (2011-0001762).

## REFERENCES

- Hobza, P.; Havlas, Z. Blue-Shifting Hydrogen Bonds. *Chem. Rev.* **2000**, *100*, 4253–4264.
- Sobolewski, A. L.; Domcke, W. Computational Studies of the Photophysics of Hydrogen-Bonded Molecular Systems. *J. Phys. Chem. A* **2007**, *111*, 11725–11735.
- Gu, Q.; Trindle, C.; Knee, J. L. Communication: Frequency Shifts of an Intramolecular Hydrogen Bond as a Measure of Intermolecular Hydrogen Bond Strengths. *J. Chem. Phys.* **2012**, *137*, 091101.
- Nagornova, N. S.; Rizzo, T. R.; Boyarkin, O. V. Interplay of Intra- and Intermolecular H-Bonding in a Progressively Solvated Macroyclic Peptide. *Science* **2012**, *336*, 320–323.
- Zelený, T.; Ruckenbauer, M.; Aquino, A. J. A.; Müller, T.; Lankás, F.; Dršta, T.; Hase, W. L.; Nachtigallova, D.; Lischka, H. Strikingly Different Effects of Hydrogen Bonding on the Photodynamics of Individual Nucleobases in DNA: Comparison of Guanine and Cytosine. *J. Am. Chem. Soc.* **2012**, *134*, 13662–13669.
- Sobolewski, A. L.; Domcke, W. Photoinduced Electron and Proton Transfer in Phenol and Its Clusters with Water and Ammonia. *J. Phys. Chem. A* **2001**, *105*, 9275–9283.
- Frutos, L. M.; Markmann, A.; Sobolewski, A. L.; Domcke, W. Photoinduced Electron and Proton Transfer in the Hydrogen-Bonded Pyridine–Pyrrole System. *J. Phys. Chem. B* **2007**, *111*, 6110–6112.
- Poterya, V.; Profant, V.; Fárník, M.; Šištík, L.; Slavíček, P.; Buck, U. Photoinduced Processes in Hydrogen Bonded System: Photo-dissociation of Imidazole Clusters. *J. Phys. Chem. A* **2009**, *113*, 14583–14590.
- Rubio-Lago, L.; Amaral, G. A.; Oldani, A. N.; Rodriguez, J. D.; Gonzalez, M. G.; Pino, G. A.; Banares, L. Photodissociation of Pyrrole–Ammonia Clusters by Velocity Map Imaging: Mechanism for the H-atom Transfer Reaction. *Phys. Chem. Chem. Phys.* **2011**, *13*, 1082–1091.
- Yang, Y. L.; Ho, Y.-C.; Dyakov, Y. A.; Hsu, W.-H.; Ni, C.-K.; Sun, Y.-L.; Tsai, W.-C.; Hu, W.-P. Effects of Intramolecular Hydrogen Bonding on the Excited State Dynamics of Phenol Chromophores. *Phys. Chem. Chem. Phys.* **2013**, *15*, 7182–7190.
- Domcke, W.; Yarkony, D. R.; Koppel, H., Eds. *Conical Intersections: Electronic Structure, Dynamics and Spectroscopy*; World Scientific: Singapore, 2004.
- Domcke, W.; Yarkony, D. R.; Koppel, H., Eds. *Conical Intersections: Theory, Computation and Experiment*; World Scientific: Singapore, 2011.
- Domcke, W.; Yarkony, D. R. Role of Conical Intersections in Molecular Spectroscopy and Photoinduced Chemical Dynamics. *Annu. Rev. Phys. Chem.* **2012**, *63*, 325–352.
- Worth, G. A.; Cederbaum, L. S. beyond Born–Oppenheimer: Molecular Dynamics through a Conical Intersection. *Annu. Rev. Phys. Chem.* **2004**, *55*, 127–158.
- Li, W.; Zhou, X.; Lock, R.; Patchkovskii, S.; Stolow, A.; Kapteyn, H. C.; Murnane, M. M. Time-Resolved Dynamics in  $N_2O_4$  Probed Using High Harmonic Generation. *Science* **2008**, *322*, 1207–1211.
- Horio, T.; Fuji, T.; Suzuki, Y.-I.; Suzuki, T. Probing Ultrafast Internal Conversion through Conical Intersection via Time-Energy Map of Photoelectron Angular Anisotropy. *J. Am. Chem. Soc.* **2009**, *131*, 10392–10393.
- Polli, D.; Altoè, P.; Weingart, O.; Spillane, K. M.; Manzoni, C.; Brida, D.; Tomasello, G.; Orlandi, G.; Kukura, P.; Mathies, R. A.; et al. Conical Intersection Dynamics of the Primary Photoisomerization Event in Vision. *Nature* **2010**, *467*, 440–443.
- Lim, J. S.; Kim, S. K. Experimental Probing of Conical Intersection Dynamics in the Photodissociation of Thioanisole. *Nat. Chem.* **2010**, *2*, 627–632.
- Worner, H. J.; Bertrand, J. B.; Fabre, B.; Higuet, J.; Ruf, H.; Dubrouil, A.; Patchkovskii, S.; Spanner, M.; Mairesse, Y.; Blanchet, V.; et al. Conical Intersection Dynamics in  $NO_2$  Probed by Homodyne High-Harmonic Spectroscopy. *Science* **2011**, *334*, 208–212.
- Yarkony, D. R. Conical Intersections: The New Conventional Wisdom. *J. Phys. Chem. A* **2001**, *105*, 6277–6293.

- (21) Yarkony, D. R. Diabolical Conical Intersections. *Rev. Mod. Phys.* **1996**, *68*, 985–1013.
- (22) Yarkony, D. R. Nonadiabatic Quantum Chemistry: Past, Present, and Future. *Chem. Rev.* **2012**, *112*, 481–498.
- (23) Sobolewski, A. L.; Domcke, W.; Dedonder-Lardeux, C.; Jouvet, C. Excited-State Hydrogen Detachment and Hydrogen Transfer Driven by Repulsive  $\pi\sigma^*$  States: A New Paradigm for Nonradiative Decay in Aromatic Biomolecules. *Phys. Chem. Chem. Phys.* **2002**, *4*, 1093–1100.
- (24) Ashfold, M. N. R.; Devine, A. L.; Dixon, R. N.; King, G. A.; Nix, M. G. D.; Oliver, T. A. A. Exploring Nuclear Motion through Conical Intersections in the UV Photodissociation of Phenols and Thiophenol. *Proc. Natl. Acad. Sci.* **2008**, *105*, 12701–12706.
- (25) Ashfold, M. N. R.; King, G. A.; Murdock, D.; Nix, M. G. D.; Oliver, T. A. A.; Sage, A. G.  $\pi\sigma^*$  Excited States in Molecular Photochemistry. *Phys. Chem. Chem. Phys.* **2010**, *12*, 1218–1238.
- (26) Ashfold, M. N. R.; Cronin, B.; Devine, A. L.; Dixon, R. N.; Nix, M. G. D. The Role of  $\pi\sigma^*$  Excited States in the Photodissociation of Heteroaromatic Molecules. *Science* **2006**, *312*, 1637–1640.
- (27) Roberts, G. M.; Williams, C. A.; Young, J. D.; Ullrich, S.; Paterson, M. J.; Stavros, V. G. Unraveling Ultrafast Dynamics in Photoexcited Aniline. *J. Am. Chem. Soc.* **2012**, *134*, 12578–12589.
- (28) Sicilia, F.; Blancafort, L.; Bearpark, M. J.; Robb, M. A. Quadratic Description of Conical Intersections: Characterization of Critical Points on the Extended Seam. *J. Phys. Chem. A* **2007**, *111*, 2182–2192.
- (29) Migani, A.; Blancafort, L.; Robb, M. A.; DeBellis, A. D. An Extended Conical Intersection Seam Associated with a Manifold of Decay Paths: Excited-State Intramolecular Proton Transfer in O-Hydroxybenzaldehyde. *J. Am. Chem. Soc.* **2008**, *130*, 6932–6933.
- (30) Paterson, M. J.; Bearpark, M. J.; Robb, M. A.; Blancafort, L.; Worth, G. A. Conical Intersections: A Perspective on the Computation of Spectroscopic Jahn–Teller Parameters and the Degenerate ‘Intersection Space’. *Phys. Chem. Chem. Phys.* **2005**, *7*, 2100–2115.
- (31) Lim, J. S.; Lim, I. S.; Lee, K.-S.; Ahn, D.-S.; Lee, Y. S.; Kim, S. K. Intramolecular Orbital Alignment Observed in the Photodissociation of  $[D_1]Thiophenol$ . *Angew. Chem., Int. Ed.* **2006**, *45*, 6290–6293.
- (32) Lim, J. S.; Choi, H.; Lim, I. S.; Park, S. B.; Lee, Y. S.; Kim, S. K. Photodissociation Dynamics of Thiophenol- $d_1$ : The Nature of Excited Electronic States along the S–D Bond Dissociation Coordinate. *J. Phys. Chem. A* **2009**, *113*, 10410–10416.
- (33) Devine, A. L.; Nix, M. G. D.; Dixon, R. N.; Ashfold, M. N. R. Near-Ultraviolet Photodissociation of Thiophenol. *J. Phys. Chem. A* **2008**, *112*, 9563–9574.
- (34) Lim, I. S.; Lim, J. S.; Lee, Y. S.; Kim, S. K. Experimental and Theoretical Study of the Photodissociation Reaction of Thiophenol at 243nm: Intramolecular Orbital Alignment of the Phenylthiyl Radical. *J. Chem. Phys.* **2007**, *126*, 034306–034310.
- (35) Venkatesan, T. S.; Ramesh, S. G.; Lan, Z.; Domcke, W. Theoretical Analysis of Photoinduced H-atom Elimination in Thiophenol. *J. Chem. Phys.* **2012**, *136*, 174312–174316.
- (36) Roberts, G. M.; Hadden, D. J.; Bergendahl, L. T.; Wenge, A. M.; Harris, S. J.; Karsili, T. N. V.; Ashfold, M. N. R.; Paterson, M. J.; Stavros, V. G. Exploring Quantum Phenomena and Vibrational Control in  $\sigma^*$  Mediated Photochemistry. *Chem. Sci.* **2013**, *4*, 993–1001.
- (37) Lim, J. S.; Lee, Y. S.; Kim, S. K. Control of Intramolecular Orbital Alignment in the Photodissociation of Thiophenol: Conformational Manipulation by Chemical Substitution. *Angew. Chem., Int. Ed.* **2008**, *47*, 1853–1856.
- (38) Oliver, T. A. A.; King, G. A.; Tew, D. P.; Dixon, R. N.; Ashfold, M. N. R. Controlling Electronic Product Branching at Conical Intersections in the UV Photolysis of para-Substituted Thiophenols. *J. Phys. Chem. A* **2012**, *116*, 12444–12459.
- (39) Eppink, A. T. J. B.; Parker, D. H. Velocity Map Imaging of Ions and Electrons using Electrostatic Lenses: Application in Photoelectron and Photofragment Ion Imaging of Molecular Oxygen. *Rev. Sci. Instrum.* **1997**, *68*, 3477–3484.
- (40) Dribinski, V.; Ossadchi, A.; Mandelshtam, V. A.; Reisler, H. Reconstruction of Abel-transformable Images: The Gaussian Basis-set Expansion Abel Transform Method. *Rev. Sci. Instrum.* **2002**, *73*, 2634–2642.
- (41) Werner, H.-J.; Knowles, P. J. A Second Order Multi-configuration SCF Procedure with Optimum Convergence. *J. Chem. Phys.* **1985**, *82*, 5053–5063.
- (42) Knowles, P. J.; Werner, H. J. An Efficient Second-Order MC SCF Method for Long Configuration Expansions. *Chem. Phys. Lett.* **1985**, *115*, 259–267.
- (43) Celani, P.; Werner, H.-J. Multireference Perturbation Theory for Large Restricted and Selected Active Space Reference Wave Functions. *J. Chem. Phys.* **2000**, *112*, 5546.
- (44) Becke, A. D. Density-Functional Exchange-Energy Approximation with Correct Asymptotic Behavior. *Phys. Rev. A* **1988**, *38*, 3098–3100.
- (45) Borrelli, R.; Peluso, A. Dynamics of Radiationless Transitions in Large Molecular Systems: A Franck–Condon-based Method Accounting for Displacements and Rotations of all the Normal Coordinates. *J. Chem. Phys.* **2003**, *119*, 8437–8448.
- (46) Peluso, A.; Santoro, F.; Re, G. D. Vibronic Coupling in Electronic Transitions with Significant Duschinsky Effect. *Int. J. Quantum Chem.* **1997**, *63*, 233–244.
- (47) Weinhold, F. Natural Bond Orbital Analysis: A Critical Overview of Relationships to Alternative Bonding Perspectives. *J. Comput. Chem.* **2012**, *33*, 2363–2379.
- (48) Werner, H. J.; et al. MOLPRO, version 2010.1, a package of ab initio programs; Cardiff University: Cardiff, U.K., 2010.
- (49) Frisch, M. J.; et al. Gaussian 09, revision A.1; Gaussian, Inc.: Wallingford, CT, 2009.
- (50) Paul, B. K.; Guchhait, N. TD-DFT Investigation of the Potential Energy Surface for Excited-State Intramolecular Proton Transfer (ESIPT) Reaction of 10-Hydroxybenzo[h]quinoline: Topological (AIM) and Population (NBO) Analysis of the Intramolecular Hydrogen Bonding Interaction. *J. Lumin.* **2011**, *131*, 1918–1926.
- (51) Reed, A. E.; Curtiss, L. A.; Weinhold, F. Intermolecular Interactions from a Natural Bond Orbital, Donor-Acceptor Viewpoint. *Chem. Rev.* **1988**, *88*, 899–926.